# Modifying Friction by Manipulating Normal Response to Lateral Motion

V. Zaloj,* M. Urbakh, and J. Klafter
*School of Chemistry, Tel Aviv University, 69978, Tel Aviv, Israel*
(Received 22 December 1998)

We investigate the coupled lateral-normal response to a lateral external drive in a nanoscale molecular system confined between two atomically smooth solid surfaces. We discuss the effects of shear induced dilatancy, which results from the coupling, on the energy dissipation, and therefore on the frictional properties. It is demonstrated that measurements of response in the normal direction provide additional information on the mechanisms of friction and that manipulating the dilatancy opens new possibilities to control the motion in the lateral direction. The dilatancy leads to a novel memory effect which is amenable to experimental verification. [S0031-9007(99)09350-3]

PACS numbers: 46.55.+d

Interfacial friction is one of the oldest problems in physics and chemistry and certainly one of the most important from a practical point of view [1]. Recently, new experimental tools have been developed that allow for detailed investigations of friction at nanometer length scales [2–4], and which have led to an increase in activity in the study of interfacial friction on the microscopic level. Intriguing dynamical features have been observed experimentally in nanoscale molecular systems, sheared between two atomically smooth solid surfaces, which include, for example, stick-slip motion, intermittent stick-slip motion characterized by force fluctuations, transition to sliding above the critical velocity, and a dependence of friction on the history of the system. These and other observations have motivated theoretical efforts [5–12], both numerical and analytical, but most issues are still subject to controversy.

While most studies of frictional forces, using surface force apparatus (SFA), have focused on the lateral response to a lateral driving force, there have been a few theoretical and experimental observations of response in the normal direction [13–16]. A feature characteristic of the response in the normal direction is the dilatancy during slippage and sliding, observed in experiments and molecular dynamics calculations. The interest in coupling between lateral and normal motions has recently gained additional attention due to the prediction that one should be able to modify the lateral response by imposing a controlling normal drive [17–20].

Here we investigate a response in the normal direction, induced by a lateral drive, in the context of SFA. Figure 1A displays schematically the basic tribological setup typical of SFA experiments, which allows for motion in both lateral and normal directions. We show that a detailed analysis of motion in the normal direction can add to our understanding of the mechanisms leading to friction, and therefore open new possibilities to control the motion in the lateral direction.

In order to demonstrate what can be obtained from considering the lateral-normal coupling, we propose a generalization of the one-dimensional Tomlinson model to include also the normal direction [21]. The one-dimensional Tomlinson model has proven powerful in describing the lateral motion of the top plate in SFA configurations and in reproducing many of the phenomena observed experimentally. Introducing lateral-normal coupling leads to the following coupled equations of motion which describe the top plate of mass $M$, which is connected to a laterally driving spring, of spring constant $K_d$,

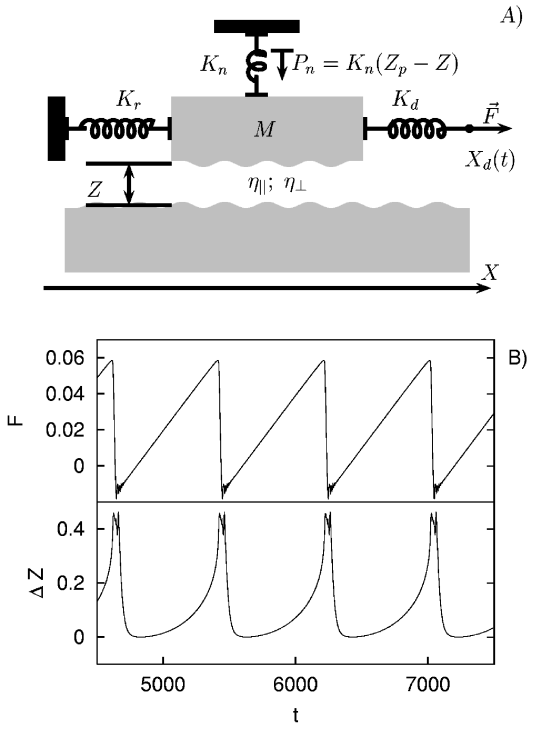


FIG. 1. (A) Schematic sketch of the model geometry; (B) the time series of the lateral force, $F = K_d[X - X_d(t)]$, and the dilatancy $\Delta Z$. The force, dilatancy, and time are presented in units of $(4\pi^2 U_0/b)$, $b$, and $1/\omega_0 = (b/2\pi)\sqrt{M/U_0}$, respectively [22]. Parameter values: $\Lambda = b$, $\eta_{\|} = 0.1M\omega_0$, $\eta_\perp = 5\eta_{\|}$, $\sqrt{(K_r + K_d)/M} = 0.1\omega_0$, $K_n = K_r + K_d$, $\sigma = 0.7$, $V = 0.01b\omega_0$, and $P_n^0 = 1.3 \times 10^{-2}(4\pi^2 U_0/b)$.

  

and to springs $K_r$ and $K_n$ which are used to measure the response in the lateral and normal directions, respectively:

$$M\ddot{X}(t) = -\eta_{\parallel}(Z)\dot{X}(t) - \partial U(X,Z)/\partial X + K_d[X_d(t) - X(t)] - K_r X(t), \quad (1)$$

and

$$M\ddot{Z}(t) = -\eta_{\perp}(Z)\dot{Z}(t) - \partial U(X,Z)/\partial Z + K_n[Z_P(t) - Z(t)], \quad (2)$$

where

$$\eta_{\parallel,\perp}(Z) = \eta^0_{\parallel,\perp}\exp(1 - Z/\Lambda), \quad (3)$$

and

$$U(X,Z) = U_0\exp(1 - Z/\Lambda)[1 - \sigma^2\cos(2\pi X/b)]. \quad (4)$$

$U(X,Z)$ is the effective potential experienced by the plate due to the presence of the embedded system, $b$ is its periodicity, and $\sigma$ characterizes the corrugation of the potential in the lateral direction. The parameters $\eta_{\parallel}$ and $\eta_{\perp}$ are responsible for the dissipation of the plate kinetic energy due to the motion in the lateral and normal directions. In contrast to the traditional Tomlinson model, here we take into account the dependence of $U$ and $\eta_{\parallel,\perp}$ on the distance $Z$ between plates. The detailed distance dependence is determined by a nature of the interaction between the plate and embedded system. As an example, we assume an exponential decrease of $U$ and $\eta_{\parallel,\perp}$ with a rate $\Lambda^{-1}$ as $Z$ increases. The coordinate of the laterally driven stage is denoted as $X_d(t)$. The possibility of an external modulation of the normal load $P_n(t) \equiv K_n[Z_P(t) - Z(t)]$ is taken into account by introducing a time dependence into the position of the normal stage, $Z_P(t)$. Using the coupled Eqs. (1) and (2) for describing the motion of the top plate is justified under the condition of separation of time scales; namely, when the response of the embedded system is faster than that of the top plate. Eqs. (1) and (2) correspond to the configuration shown schematically in Fig. 1A.

A relevant property of the coupled equations is the existence of two stable surface separations $Z_0$ and $Z_S$, which correspond to the plate being either at rest or in fast motion. At rest the plate feels the lateral corrugation of the potential, $U(X,Z)$, and sits at the minima of the potential, while during fast motion there is a decoupling from this potential corrugation. From Eqs. (1) and (2), together with $U(X,Z)$ in Eq. (4) one obtains the following equation for the maximal dilatancy:

$$\Delta Z_D = Z_S - Z_0 = (P^0_n/K_n)[(1 - \sigma^2)^{-1}\exp(-\Delta Z_D/\Lambda) - 1], \quad (5)$$

where $P^0_n = (1 - \sigma^2)(U_0/\Lambda)\exp(1 - Z_0/\Lambda)$ is the normal load at rest. Equation (5) demonstrates that the dilatancy $\Delta Z_D$ explicitly depends on the potential corrugation and on the normal spring constant. It is quite evident that measuring the dilatancy helps in determining the amplitude of the potential corrugation. This stems from the additional information due to the two limiting behaviors in the normal direction.

Figure 1B shows the response in the lateral and normal directions to a lateral constant velocity drive, given by $X_d(t) = Vt$ in Eq. (1), and which is applied in tribological studies. Figure 1B corresponds to the stick-slip regime that occurs at low driving velocities [13,16]. The separation between the plates, which is initially $Z_0$, at equilibrium, starts growing before slippage occurs and stabilizes at a larger interplate distance as long as the motion continues. Since the static friction is determined by the amplitude of the potential corrugation $\sigma^2 U_0\exp(1 - Z/\Lambda)$, it is obvious that the dilatancy leads to a decrease of the static friction compared to the case of a constant distance between plates. The time series in Fig. 1B can be understood in terms of the two states (rest and fast motion) that are characteristic of stick-slip motion. Namely, dilatancy is expected in a broad range of systems where coupling between lateral and normal directions exists. Its observation is limited by the choice of the normal spring which should be weaker than the potential elasticity, $K_n\Lambda^2 \ll U_0$.

In the sliding regime, which occurs for driving velocities higher than a critical velocity $V_c$, the fluctuations in the normal direction become negligible and the interplate distance remains at $Z_S$. This distance, and correspondingly the viscous frictional force, $F_v = \eta_{\parallel}(Z_S)V$, as well as the static friction, depend on the normal load.

Two approaches are used usually to investigate shear forces in confined liquids: the tribological one, where a constant driving velocity is applied, as discussed above, and the rheological one, which applies an oscillatory external drive $X_d(t) = X_{0d}\sin(\omega_d t)$ [22,23]. When an oscillatory drive is applied, the response of the system is analyzed in terms of complex dynamic moduli. The rheological analysis of the moduli allows one to distinguish between elastic and viscous components of the interactions. Here we concentrate on the viscous part, which is directly related to the energy dissipation, and therefore to the effective viscosity [22]. Figure 2 presents the effective viscosity, $\eta_{\text{eff}}$, lateral frictional force, $F_v$, and the corresponding friction coefficient, $\mu$, as a function of the top plate velocity, for various normal loads. The velocity has been introduced to display the rheological measurements, and is defined as $V = X\bar{\omega}_d$, where $\bar{X}$ is the amplitude of the top plate displacement and $\omega_d$ is the driving frequency [22]. The results in Fig. 2 have been obtained by fixing $\omega_d$ and varying the amplitude $\bar{X}$, which is the usual experimental procedure.

The main feature in Fig. 2 is the discontinuous transition from local motion, where the top plate displacement is smaller than the period of the surface potential, to a large scale response, where the top plate executes displacements larger than the potential period. The large scale response includes the stick-slip and sliding regimes.

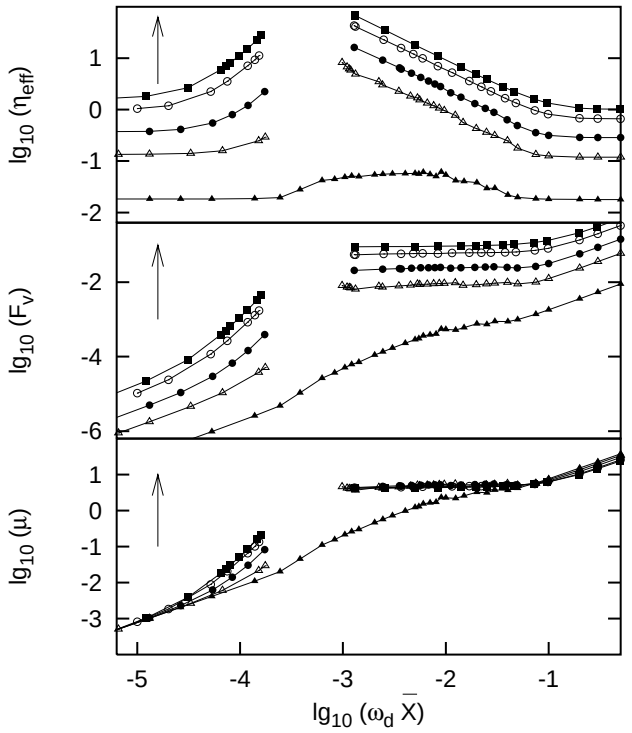


FIG. 2. The dimensionless effective viscosity, $\eta_{\rm eff}$, frictional force $F_{\rm v}$, and friction coefficient $\mu = F_{\rm v}/P_n^0$ as a function of the top plate velocity for an oscillatory drive. Calculations have been done for different normal loads, $P_n^0$; the arrows indicate the direction of the increasing load. From bottom to top: $P_n^0 = 2.4 \times 10^{-4}$, $1.8 \times 10^{-3}$, $4.8 \times 10^{-3}$, $1.3 \times 10^{-2}$, and $2.1 \times 10^{-2}$ in units of $(4\pi^2 U_0/b)$. Parameter values as in Fig. 1; except $\eta_{\parallel} = M\omega_0$ and $\omega_d = 10^{-3}\omega_0$.

The discontinuous transition does not appear for low normal loads when there is no stick-slip regime. With an increase in the normal load the effective interaction experienced by the plate increases and the transition becomes more pronounced. The rheological response shown in Fig. 2 is typical to nanoscale lubricated systems [15]. It has been suggested that the dramatic changes in the effective viscosity with varying normal load, as shown in Fig. 2, are induced by a phase transition in the embedded system [4]. Our calculations demonstrate that this effect can be explained as a dynamical phase transition due to the competition between the elasticity of the effective potential and the driving spring.

Interestingly, in the local response regime the system exhibits *shear thickening* where $\eta_{\rm eff}$ increases with increasing velocity; see Fig. 2. This reflects the existence of an additional channel of dissipation which originates from the oscillations in the normal direction. The excitation of normal oscillations by the lateral drive becomes efficient only when the amplitude of the lateral oscillations is large enough to feel a nonlinearity of the potential $U(X, Z)$. As a result, the dilatancy and additional energy dissipation due to normal motion occur only for driving velocities which exceed some critical value which depends on the load. These features of the lateral-normal coupling have been observed recently in SFA experiments [15,16].

The middle panel of Fig. 2 displays the lateral frictional force, $F_{\rm v}$, as a function of the velocity for different loads, and again has a discontinuous jump between local and nonlocal motions. Our calculations show that in the range of stick-slip motion the frictional forces remain constant, independent of velocity. This solidlike behavior has been observed for nanoscale lubricated systems [15,16]. When defining the friction coefficient, $\mu = F_{\rm v}/P_n^0$, we notice that the curves belonging to different loads collapse into a single curve, except for low normal loads, where the system does not exhibit solidlike behavior. This supports the usefulness of the concept of friction coefficient [1]. From Fig. 2 we conclude that the textbook term of friction coefficient holds only over a limited range of velocities, where it is independent of velocity.

Dilatancy has been shown above to occur naturally during slippage events. It has also been demonstrated that the measured frictional forces are sensitive to the interplate distance. One can therefore expect to be able to control frictional behavior by monitoring the motion in the normal direction. Controlling frictional forces has been traditionally approached by chemical means, namely, using lubricating liquids. A different approach, proposed here, is by controlling the system mechanically. Our goal is twofold: (a) to achieve smooth sliding at low driving velocities, which otherwise correspond to the stick-slip regime; (b) to decrease the frictional forces [17].

We introduce two approaches to control friction by mechanical means, which differ from the feedback method proposed earlier [17]. From the dependence of the dilatancy $\Delta Z_D$ on the normal spring constant $K_n$, given by Eq. (5), it is clear that the weaker $K_n$ is the larger $\Delta Z_D$ is and therefore the frictional force tends to decrease. Figure 3 displays the lateral and normal responses for

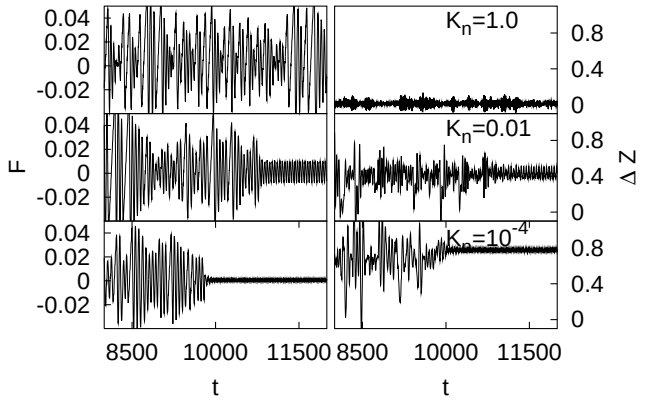


FIG. 3. The time series of the lateral force, $F$, and dilatancy, $\Delta Z$, for given driving velocity and normal load, but for different strengths of the normal spring, $K_n$. With a decrease in the stiffness of the normal spring there is an increase in the interplate distance $\Delta Z$. Parameter values as in Fig. 1; except $\eta_{\parallel} = 10^{-2} M\omega_0$ and $V = 0.11 b\omega_0$.

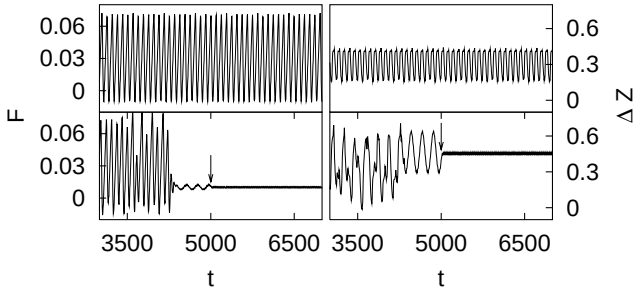


FIG. 4. The applied sinusoidal perturbation, $Z_p(t) = Z_p^0 + \Delta Z_p \sin(\omega_n t)$, is of an amplitude $\Delta Z_p = 0.5b$ and a frequency, $\omega_n = 3.1 \times 10^{-2}\omega_0$, smaller than the resonant frequency in the normal direction. The driving velocity and the average load are the same as in the top panel. The arrow indicates the time when the normal perturbation is turned off. The driving velocity $V = 0.15b\omega_0$.

different normal spring constants, while all other parameters are kept fixed. We see that as the spring constant $K_n$ decreases the dilatancy grows, which leads to smoothing of the stick-slip motion present for stiffer springs. Weakening the spring constant results in lowering the critical velocity at which stick-slip turns to sliding. This approach should be applicable for underdamped conditions, when $\eta_{\parallel,\perp}^2 \ll M(K_d + K_r)$. It also emphasizes that the experimental observations in SFA strongly depend on the choice of the mechanical parameters.

For overdamped conditions a different method of control can be applied by adding external oscillations to the normal load using a sinusoidal drive $Z_P(t)$ in Eq. (2). Figure 4 shows that the effect of these oscillations in smoothing the stick-slip behavior is correlated with the growing of the dilatancy. The smoothing in this case originates from a bistability in the system in the vicinity of the critical velocity. The external oscillations force the plate into a sliding state which corresponds to a larger dilatancy. The sliding state is only locally stable below the critical velocity in the absence of the oscillations. Normal oscillations push the system into the region of attraction of this state (limit cycle) and it remains trapped there even when the oscillations are turned off (steady state). Namely, the dilatancy introduces a long range memory effect which is a manifestation of the stability of the sliding state even below the critical velocity. This memory effect is amenable to verification in stop-start experiments [24]. In real systems one expects metastability rather than stability of the sliding states.

We have explored a wide range of system parameters to better understand the range of possible behaviors. Experimental conditions usually correspond to the overdamped limit with respect to the external springs, $K_d$, $K_r$, and $K_n$, and underdamped with respect to the effective interaction $U_0$.

Financial support for this work by the Israel Science Foundation, the GIF, and DIP grants is gratefully acknowledged.

*Permanent address: Department of Physics, State University of Moldova, Mateevici Strasse 60, MD-2009, Chişinau, Republic of Moldova.

[1] F. P. Bowden and D. Tabor, *The Friction and Lubrications of Solids* (Clarendon Press, Oxford, 1985).
[2] H. Yoshizawa, P. McGuiggan, and J. Israelachvili, Science **259**, 1305 (1993).
[3] H.-W. Hu, G. A. Carson, and S. Granick, Phys. Rev. Lett. **66**, 2758 (1991).
[4] J. Klein and E. Kumacheva, Science **269**, 816 (1995).
[5] P. A. Thompson, M. O. Robbins, and G. S. Grest, Isr. J. Chem. **35**, 93 (1995).
[6] M. G. Rozman, M. Urbakh, and J. Klafter, Phys. Rev. Lett. **77**, 683 (1996).
[7] J. M. Carlson and A. A. Batista, Phys. Rev. E **53**, 4153 (1996).
[8] Y. Braiman, F. Family, and G. Hentschel, Phys. Rev. B **55**, 5491 (1996).
[9] J. P. Gao, W. D. Luedtke, and U. Landman, Phys. Rev. Lett. **79**, 705 (1997).
[10] M. G. Rozman, M. Urbakh, J. Klafter, and F.-J. Elmer, J. Phys. Chem. **102**, 7924 (1998).
[11] B. N. J. Persson, *Sliding Friction, Physical Properties and Applications* (Springer-Verlag, Berlin, 1998).
[12] T. Baumberger and C. Caroli, Eur. Phys. J. B **4**, 13 (1998).
[13] S. Nasuno, A. B. A. Kudrolli, and J. P. Gollub, Phys. Rev. E **58**, 2161 (1998).
[14] P. A. Thompson and G. S. Grest, Phys. Rev. Lett. **67**, 1751 (1991).
[15] A. L. Demirel and S. Granick, J. Chem. Phys. **109**, 6889 (1998).
[16] G. Luengo, F.-J. Schmitt, R. Hill, and J. Israelachvili, Macromolecules **30**, 2482 (1997).
[17] M. G. Rozman, M. Urbakh, and J. Klafter, Phys. Rev. E **57**, 7340 (1998).
[18] F. J. Elmer, Phys. Rev. E **57**, R4903 (1998).
[19] J. P. Gao, W. D. Luedtke, and U. Landman, J. Phys. Chem. B **102**, 5033 (1998).
[20] M. Heuberger, C. Drummond, and J. Israelachvili, J. Phys. Chem. B **102**, 5038 (1998).
[21] G. A. Tomlinson, Philos. Mag. **7**, 905 (1929).
[22] V. Zaloj, M. Urbakh, and J. Klafter, Phys. Rev. Lett. **81**, 1227 (1998).
[23] V. Zaloj, M. Urbakh, and J. Klafter, J. Chem. Phys. **110**, 1263 (1999).
[24] H. Yoshizawa and J. Israelachvili, J. Phys. Chem. **97**, 11300 (1993).